Surface Properties of Elastomeric Polypropylenes Studied with Atomic Force Microscopy

C. Dietz,*,† M. Zerson, C. Riesch, M. Franke, and R. Magerle*,‡

Chemische Physik, Technische Universität Chemnitz, Reichenhainer Str. 70, 09107 Chemnitz

Received June 3, 2008; Revised Manuscript Received September 19, 2008

ABSTRACT: The energy dissipated between tip and sample during dynamic atomic force microscopy (AFM) is a sensitive measure of local surface properties. We mapped the surface properties of crystalline and amorphous regions in thin films of different kinds of elastomeric polypropylene (ePP) with 10 nm lateral resolution. The dissipated energy as a function of the amplitude setpoint displays discriminative shapes for both polymer regions. Differences in the shape as well as in the maximum amount of dissipated energy are interpreted as different amounts of amorphous material on top of crystalline regions. Indentation experiments at different amplitude setpoints resulted in indentation depths of the AFM tip up to 11 nm, on both crystalline and amorphous regions. This and the change of dissipated energy upon wet chemical etching indicate that crystalline regions are covered by an up to 10 nm thick amorphous layer.

1. Introduction

Polyolefins such as elastomeric polypropylene[1] (ePP), a semicrystalline polymer, receive increasing attention in material sciences due to their comparatively simple synthesis and their elastomeric properties. Mechanical properties of polymer surfaces play an important role in applications such as adhesives[2−4] as well as for the haptic and tribological properties of the material.[5,6] Information about the surface properties of a material could help designing new applications. The interface to air plays also an important role in structure formation processes at the surface. Extrapolating physical parameters of the bulk material is in most cases not a proper method for understanding the surface properties. An example for these difficulties is the discussion about the glass transition temperature at the surface and in thin films.[7−9]

Atomic force microscopy (AFM)[10−13] and particularly its dynamic methods[14] turned out to be a suitable instrument for investigating surfaces of a wide range of materials and multicomponent polymers in particular.[12,15−19] Force-displacement curves and the application of the AFM tip as a nanoindenter made it possible to measure elastic properties and other surface parameters.[20−23] Tao et al.[24] and Radmacher et al.[25] used this principle to determine mechanical surface properties of biological materials. Using microspheres instead of sharp AFM tips for the indentation local strains of the surface of soft materials can be avoided.[4] In this context, mathematical and physical models have been developed to assess the Young's modulus and other mechanical material properties.[26−33]

Recently, dynamic AFM methods have been developed to determine surface properties quantitatively. Based on the relationship between tip−sample energy dissipation E_{dis} and phase shift ϕ between the cantilever's oscillation and excitation,[34,35] García et al.[36] have proposed a method for identifying dissipation processes at the nanoscale. Measuring amplitude-phase-distance (APD) curves, calculating the dissipated energy per oscillation cycle by

$$E_{dis} = E_{ext} - E_{med} = \frac{\pi k A}{Q}\left(A_0 \sin\phi - \frac{A\omega}{\omega_0}\right) \quad (1)$$

and plotting these values as a function of the oscillation amplitude with respect to the free amplitude A/A_0 results in characteristic energy dissipation curves.[36] In this equation, E_{ext} and E_{med} are the excitation energy and the energy dissipated into the medium, respectively, k is the force constant, Q is the quality factor of the cantilever, ω is the excitation frequency, and ω_0 is the cantilever's resonance frequency. The shape of those curves and particularly their derivative can reveal the dissipation mechanism between the AFM tip and the sample and hence the dominant type of interaction force as recently demonstrated on silicon, on polystyrene in a polystyrene/polybutadiene blend,[36] and on elastomeric polypropylene.[19] In ref 36, three different types of interaction mechanisms between tip and sample were considered: surface energy hysteresis, long-range interfacial interactions for a silicon surface, and viscoelasticity for polystyrene.

In the present study, we apply this methodology to different kinds of ePP, which only vary in the degree of crystallinity and chain length. We map the local surface properties of crystalline and amorphous regions of ePP with 10 nm lateral resolution. Sakai et al.[37] claim the presence of an amorphous layer on top of crystalline regions at the surface of isotactic polypropylene. With successive etching we have recently confirmed the presence of such an amorphous layer.[19] Moreover, APD measurements offer the opportunity to determine the indentation depths of the AFM tip into the polymer.[33,38] In this work, we present a systematic study of energy dissipation on ePP and tip indentation into the sample surface.

2. Experimental Section

Materials. We studied three different kinds of elastomeric polypropylene (ePP) samples ePP26, ePP30, and ePP36 with weight-average molecular weights of M_w = 153, 110, and 160 kg mol^{-1}, respectively.[1] In this article the samples are signified with respect to the [*mmmm*]-pentade (*m* = meso conformation) contents. ePP26, ePP30, and ePP36 correspond to a [*mmmm*]-pentade content of 26%, 30% and 36%, respectively. The crystallinity of the samples in the bulk depends on the [*mmmm*]-pentade content.[39] From the interpolation of the data in ref 39. We determined crystallinities of 12% (ePP26), 15% (ePP30), and 20% (ePP36). The area fraction covered by crystalline regions at the sample surface was slightly above those values which are typical for the bulk material. The width of individual crystalline lamella is about 7 nm for the γ-modification and 14 nm for the α-modification at 300 K estimated by WAXS measurements.[40] The samples used in this work show (on average) an apparent lamella width of ∼14 nm on the surface. The broadening is attributed to tip convolution occurring in AFM.

* Authors to whom correspondence should be addressed.
† E-mail: christian.dietz@physik.tu-chemnitz.de.
‡ E-mail: robert.magerle@physik.tu-chemnitz.de.

10.1021/ma801236p CCC: $40.75 © 2008 American Chemical Society
Published on Web 11/07/2008

Therefore, differences in width could not be detected. In our study, we focus on ePP36 which is the sample with the largest degree of crystallinity in order to properly access both of the distinctive polymer regions with the AFM tip. For comparison we also show results obtained on ePP26 and ePP30. The storage modulus and loss modulus of the ePP samples in the bulk at 300 kHz was found to be $\sim 10^6$ Pa and $\sim 10^5$ Pa, respectively, by Carlson et al.[41]

Sample Preparation. All samples were dip-casted from a 5 mg/mL ePP solution in decaline onto a gold coated silicon substrate resulting in thin films with a thickness of ~150 nm. Film thicknesses were determined with the AFM after scratching the film as described elsewhere.[16] In most cases, samples were used for measurements one day after preparation and were never older than 5 weeks. Within this period of time no changes of the surface properties were observed. For the etching experiments, we successively removed thin layers of ~ 10 nm thickness of the polymer by wet-chemical etching with a solution of 50 mg/mL potassium permanganate in 30 wt % sulfuric acid for one minute followed by rinsing first with 10 wt % sulfuric acid and then with hydrogen peroxide, distilled water, and finally with acetone. After etching, the sample was remounted into the AFM and the position of interest was imaged.

Atomic Force Microscopy. For all measurements we used a Nanowizard I AFM (JPK Instruments AG, Berlin, Germany) and standard silicon cantilevers (Pointprobe NCH, NanoWorld AG, Neuchâtel, Switzerland) with resonance frequencies $\omega_0 \sim 284$ kHz, quality factors $Q \sim 200$, spring constants $k \sim 9.5$ N/m, and tip radii of approximately 10 nm, at a free amplitude of $A_0 \approx 35-40$ nm. For calibrating the cantilever's free amplitude, amplitude-distance curves were measured on a material (usually silicon) which is assumed to be stiff enough to resist tip indentation. The inverse slope of the amplitude decrease with decreasing tip−sample distance gives the calibration factor. For comparison the cantilever calibration was also determined with the method reported in ref 42, which gave the same results. The spring constants k of the AFM cantilevers were determined from measurements of the resonance frequency ω_0 and the quality factor Q using a method of Sader et al.[32] APD curves were measured by oscillating the AFM cantilever at its flexural resonance frequency while the AFM tip approaches the sample surface at a vertical rate of 2 Hz. The oscillation amplitude A and the phase shift ϕ between excitation and oscillation were recorded during approaching and retracting. The approach data were used to calculate the dissipated energy by applying eq 1. Measurements were accomplished under ambient conditions. In this work, values for the phase shift ϕ were treated in their original physical sense and not by the convention of the manufacturer of the AFM used in this work. Therewith, a cantilever driven at its resonance involves a phase lag of $\phi = 90°$ between the excitation signal of the driving piezo and the actual AFM tip movement. Phase lags above 90° correspond to an AFM measurement performed in the attractive and values below 90° in the repulsive regime.[14,43]

3. Results and Discussion

3.1. Distribution of Measured Dissipation Curves. Figure 1a shows an AFM phase image measured on a thin film of ePP36. In Figure 1b, the dissipated energy is plotted as a function of the cantilever's oscillation amplitude for 100 points located along one line with a lateral distance between two adjacent points of 10 nm indicated by the dashed line across the specimen in the phase image of Figure 1a. The two crosses mark the positions where the lowest (left cross) and the topmost (right cross) energy dissipation curves of Figure 1b were measured. Curves with a maximum larger than 120 eV were measured on amorphous regions. At an amplitude ratio $A/A_0 = 0.5$ a maximum dissipated energy of 160 eV was measured on amorphous regions which is about 20% of the free oscillation energy of the cantilever-tip ensemble. The curves depict the typical shape when viscoelastic forces dominate the dissipation process between AFM tip and sample.[36] Most of the curves shown in Figure 1b fall in this category since the total area of amorphous regions on the sample surface is substantially larger

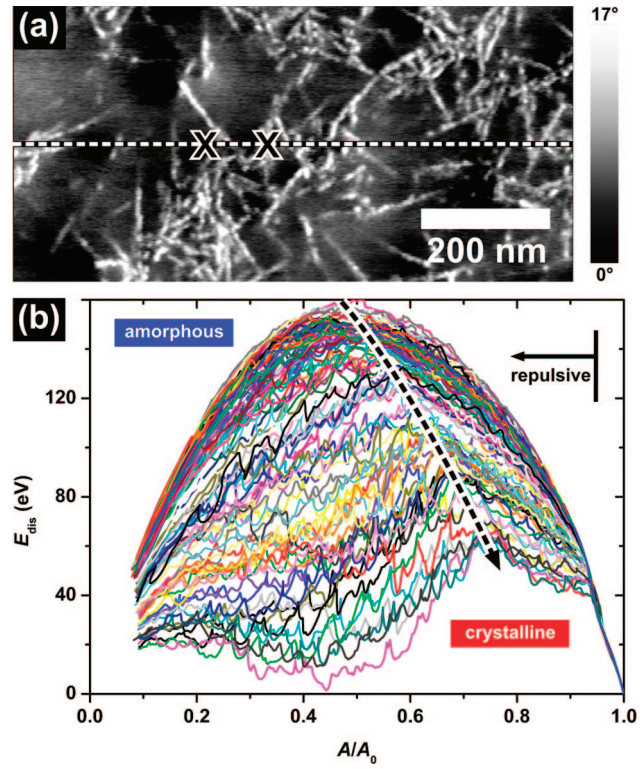

Figure 1. (a) AFM phase image of an ePP36 sample. Bright (dark) corresponds to crystalline (amorphous) regions. (b) Distribution of energy dissipation curves measured on amorphous and crystalline regions of ePP36. Each curve in the diagram represents one dissipation curve measured pointwise along the dashed line shown in part a. The smaller the maximal dissipated energy $E_{dis,max}$ is the more central the tip was located on a crystalline region. The energy dissipation curves with a maximum larger than 120 eV correspond to measurements on amorphous polymer regions.

than that of the crystalline. On the latter ones, the shape of the dissipation curves as well as the maximum amount of dissipated energy was strongly dependent on how close the AFM tip was located to the center of the crystalline region during the APD measurement. The more central the tip was located on a crystal the lower was the maximum amount of dissipated energy and the larger was the deviation from curves obtained on amorphous regions. The energy dissipation determined from APD curves measured at about 50 different positions on amorphous regions scattered by 10%. On crystalline regions the scatter was about 40%. On these regions the energy dissipation curves display a kink (see Figure 1b) which becomes more distinctive and acute-angled, the smaller the maximum value of E_{dis} was. A clear trend is visible for the maximum amount of dissipated energy highlighted by the dashed line with the arrow in the diagram of Figure 1b. The position of the local maximum shifts to higher amplitude setpoint ratios A/A_0 and to a lower dissipated energy the closer to a crystalline region of the polymer the curve was measured. For the lowest curve in the diagram the dissipated energy reduces to only 10 eV at amplitude ratios between $A/A_0 \approx 0.3-0.5$. This is attributed to a higher stiffness of the crystalline regions compared to the amorphous regions. Hence, nonconservative interactions between AFM tip and sample surface become negligible for the damped cantilever oscillation compared to the viscoelastic forces acting on amorphous regions.[44] The energy present in the cantilever-sample system is transferred from the cantilever to the sample and back to the cantilever during one oscillation cycle with only little loss of energy in terms of dissipation.

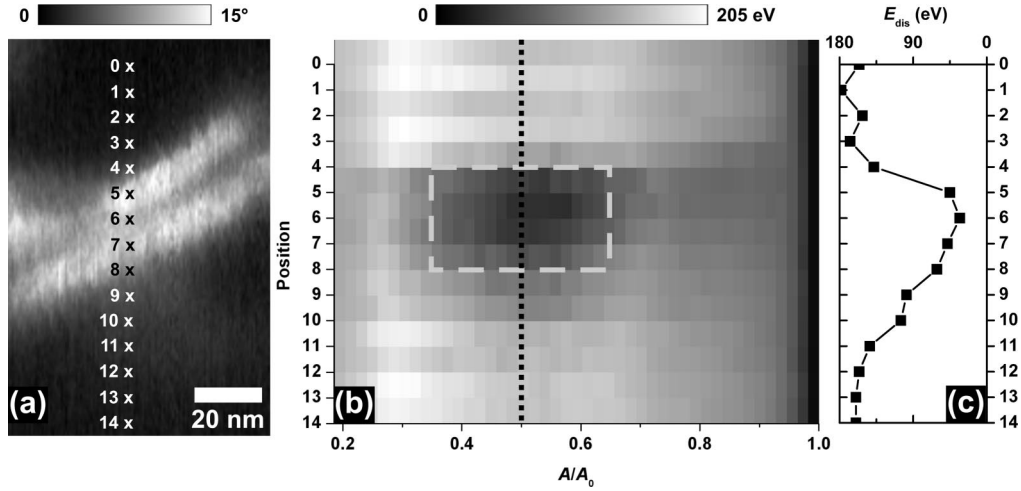

Figure 2. (a) AFM phase image of two crystalline lamellae (bright) embedded into the amorphous region (dark) of ePP36 measured at an amplitude ratio $A/A_0 = 0.67$. The numbered crosses indicate the positions where APD curves were measured. (b) Corresponding gray scale map of the dissipated energy. Each horizontal line represents an energy dissipation curve at the indicated position with the dissipated energy plotted as gray scale versus the amplitude ratio A/A_0. (c) Dissipated energy as a function of the position at an amplitude ratio $A/A_0 = 0.5$ (corresponding to the dotted line in part b).

3.2. Detection of an Individual Crystal through Energy Dissipation. We applied the same technique in the vicinity of an individual crystalline lamella in ePP36. Figure 2a shows an AFM phase image with 15 crosses marking the positions where APD curves were measured. In order to gather all information obtained from the measurement in a single diagram, we converted the dissipated energy into gray scale values and plotted them as a map with the position where the APD curve was measured as ordinate and the amplitude ratio A/A_0 as abscissa. The map clearly exhibits a decline in dissipated energy for amplitude ratios A/A_0 between 0.35 and 0.65 (marked by the dashed frame in Figure 2b) exactly at positions (black crosses in Figure 2a) where crystalline material is present. Small deviations in the position may arise from thermal drift during the measuring process. For all other setpoint ratios outside of the marked frame, however, the different polymer regions can hardly be distinguished. Additionally, the diagram reveals a maximum difference in the amount of dissipated energy between amorphous and crystalline regions for a setpoint ratio $A/A_0 \approx 0.5$. Energy dissipation curves measured on other specimens confirm this observation (see section 3.5). Figure 2c shows the amount of dissipated energy as a function of the position at the amplitude ratio $A/A_0 = 0.5$. The values vary between 180 eV on amorphous regions and 30 eV on the crystalline regions of ePP corresponding to a difference in dissipated energy of $\Delta E_{dis} = 150$ eV. Thus, the shape of the curve (E_{dis} vs position) reflects the lateral distribution of differences in the sample stiffness.

3.3. Indentation Experiments on Polypropylene. For further investigations of the surface properties of elastomeric polypropylene, we determined the indentation depth of the AFM tip into the polymer surface using the method of Höper et al.[33] and Knoll et al.[38] Figure 3a shows a typical amplitude-phase distance curve obtained on a compliant material as studied in this work and for a infinitely stiff material. The black curve (left scale) corresponds to the oscillation amplitude of the cantilever whereas the red curve belongs to the phase shift between excitation and the tip's oscillation (right scale) dependent on the tip−sample separation. The position z_0 where the AFM tip touches the sample surface for the first time is assumed to be at that point where the phase shift between the cantilever oscillation and its excitation starts to increase to higher values (above 90°) during the approach, i.e., where the attractive regime starts to dominate (Figure 3a). We would like to emphasize that this assumption is only valid for free amplitudes

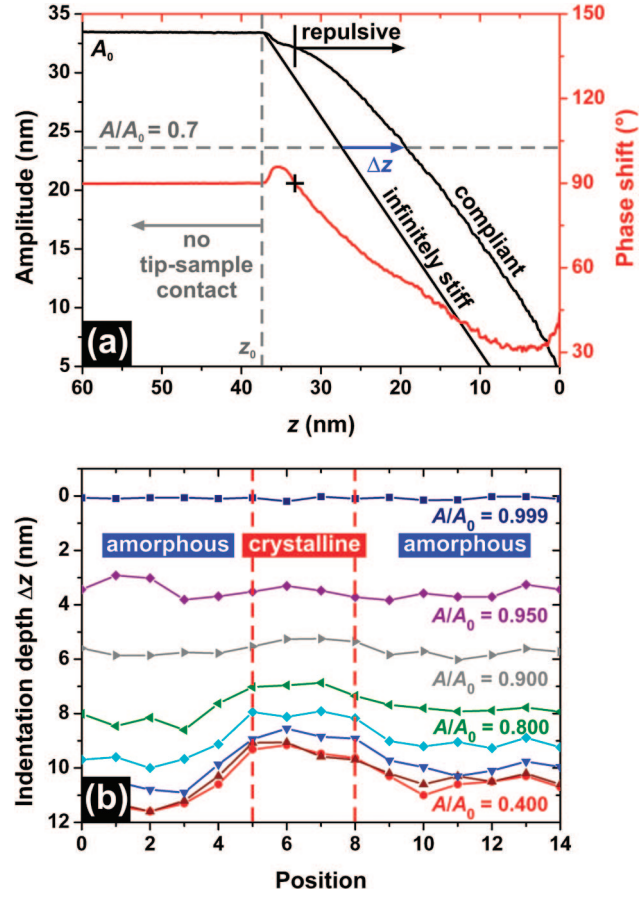

Figure 3. (a) Amplitude-phase-distance (APD) curves for an ePP36 (compliant) sample and an infinitely stiff sample. z_0 marks the onset of the attractive regime. It is the position where mechanical contact between AFM tip and sample surface occurs for the first time while approaching the surface (i.e., moving from left to right in the diagram). Δz is the indentation depth of the AFM tip into the polymer surface with respect to an infinitely stiff sample, shown for $A/A_0 = 0.7$. (b) Indentation depth Δz versus the position where APD curves were taken for different amplitude ratios $A/A_0 = 0.999$, 0.950, 0.900, 0.800, 0.700, 0.600, 0.500, and 0.400. The dashed lines enclose the area of the measurement where the crystalline region is observed in the AFM phase image. The positions where APD curves were measured correspond to that shown in Figure 2.

A_0 larger than $\sim$ 10 nm[14,43] which is the case for the range of free amplitudes (35−40 nm) used in our experiments. z_0 is the largest tip−sample separation, where the derivative of the phase shift with respect to the z-position of the piezo scanner is larger than 0.1°/nm. On an infinitely stiff sample (without any indentation) the amplitude of the oscillating cantilever would be reduced by the same amount as the z-position of the piezo scanner shifts toward the sample, resulting in a linear decrease in amplitude. At a given setpoint the distance in z-direction between the amplitude-distance curve measured on the compliant ePP sample and the assumed amplitude-distance curve of an infinitely stiff sample is the indentation depth Δz of the AFM tip into the sample surface (Figure 3a). We analyzed the APD measurements across the crystalline region (shown in Figure 2a). For each APD curve indentation depths were calculated at different amplitude ratios A/A_0 ranging from 0.999 to 0.400 and plotted versus the lateral position at the sample surface (Figure 3b). For $A/A_0 \geq 0.9$, the indentations are smaller than 6 nm and deviate less than 1 nm between amorphous and crystalline regions. Larger differences (up to 3 nm at $A/A_0 = 0.4$) are observed only for $A/A_0 \leq 0.8$. The indentation depth reaches values up to 11 nm on the amorphous region at an amplitude ratio of $A/A_0 = 0.4$. Moreover, the observation of similar indentation depths on both types of polymer regions is a further indication for the existence of an amorphous layer on top of crystalline regions of ePP36. It corroborates our earlier findings[19] and that of ref 37. We conclude that the AFM tip has first to indent into an about 7 nm thick amorphous top layer present at the whole sample surface, before crystals beneath this layer induce a notable resistance against further penetration. At this point, we would like to emphasize that an individual crystal at a polypropylene surface can be resolved more precisely and at considerably higher amplitude ratios by calculating the amount of dissipated energy per oscillation cycle between AFM tip and sample surface (Figure 2, parts b and c) than by considering the indentation depths. The thin amorphous layer screens the interaction between the AFM tip and the material beneath it. Together with the limitation of the lateral resolution due to the AFM tip radius the individual crystalline lamellae appear broader than their natural width.[16,31,40]

An alternative method for measuring the tip indentation depth is to measure the height profile of a scratch in a thin film with respect to the substrate with different amplitude ratios A/A_0. Since on the solid substrate the indentation is approximately independent of A/A_0,[38] differences in the apparent step height correspond to the tip indentation. The measured height difference between the polymer surface of ePP36 and the gold coated substrate remained constant within 1 nm while decreasing A/A_0 from 0.9 to 0.4. In contrast, the indentation depth determined from APD measurements increased from 6 to 11 nm when decreasing A/A_0 from 0.9 to 0.4 (Figure 3b). This observation gives rise to the notion that the contact mechanics of the tapping mode AFM during scanning is fundamentally different from the one prevailing during the stationary approach of the tip by accomplishing an APD curve. We attribute the main difference to the hydrodynamic buoyancy caused by the lateral motion of the AFM tip.

3.4. Successive Wet-Chemical Etching. Figure 4(a) shows the dissipation curves of ePP36 before and after successive steps of wet-chemical etching during a nanotomography experiment.[19] On average 10 nm thick layers were removed during one etching step and the APD curves were measured after several etching steps. The upper five curves enclosed by the blue bracket correspond to the dissipation curves obtained on an amorphous region of ePP before ablation, and after 1, 5, 10, and 15 etching steps, respectively. The lower curves marked with the red bracket were measured on crystalline regions, correspondingly.

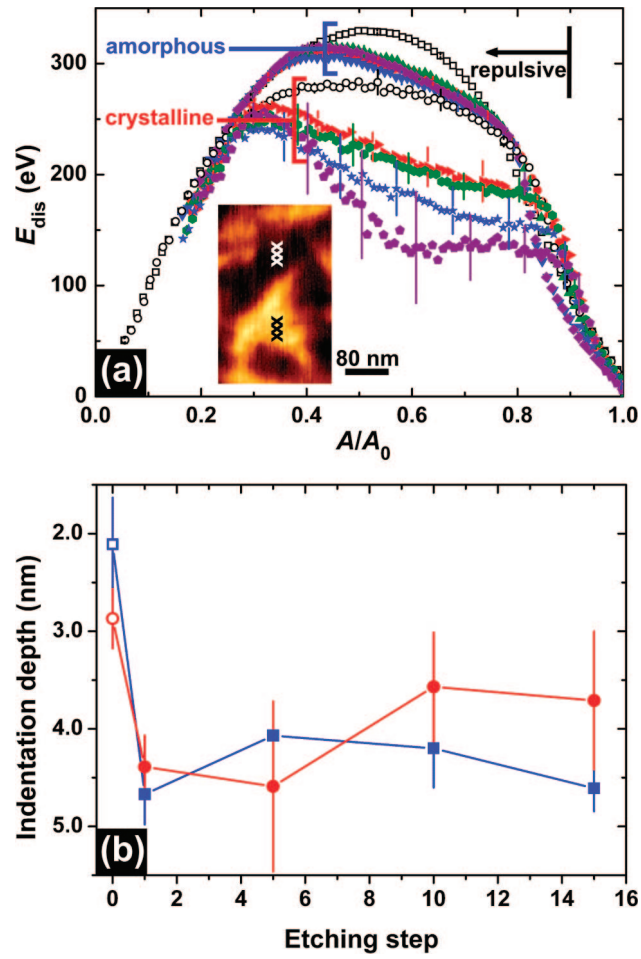

Figure 4. (a) Averaged dissipation curves measured on amorphous and on crystalline regions of ePP36 before (open symbols) and after 1, 5, 10, and 15 etching steps (closed symbols, red, green, blue, and purple, respectively). The inset shows the corresponding phase image (phase range 0−31°). The positions where APD curves were measured are marked with crosses. The black arrow indicates the transition from the attractive to the repulsive regime. For clarity, error bars are only shown for every tenth data point. (Reprinted with permission from ref 19. Copyright 2008 The American Institute of Physics). (b) Averaged indentation depth on amorphous (blue dots) and crystalline regions (red dots) at a setpoint ratio $A/A_0 = 0.5$ before etching (open symbols) and after 1, 5, 10 and 15 etching steps (closed symbols), respectively.

The data points were obtained by averaging three energy dissipation curves of each polymer region measured at the positions indicated by crosses in the inset. The corresponding standard deviation is indicated by the error bars for every tenth data point. On the amorphous region, the curves measured after the first and the subsequent etching steps were all very similar to the curve measured prior to etching. The variation was within the scatter mentioned above. The shape of the curves resembled a dissipation process in which viscoelastic forces between tip and sample prevail.[36] The slight decrease in the maximum amount of energy can be ascribed to a change of the tip apex which is likely to become blunter during the measurement. There was no drastic change neither in the amount of energy dissipation nor in the shape of the curves. Thus, we concluded that the mechanical properties on amorphous regions of the surface were not significantly altered during etching. The dissipation curve measured on the crystalline region before etching was very similar to dissipation curves measured on the amorphous regions. After the first etching, the curve shape corresponding to the crystalline region changed and the maximum amount of dissipated energy decreased by about $^1/_3$. We attribute this effect to a decrease of viscoelastic dissipation and

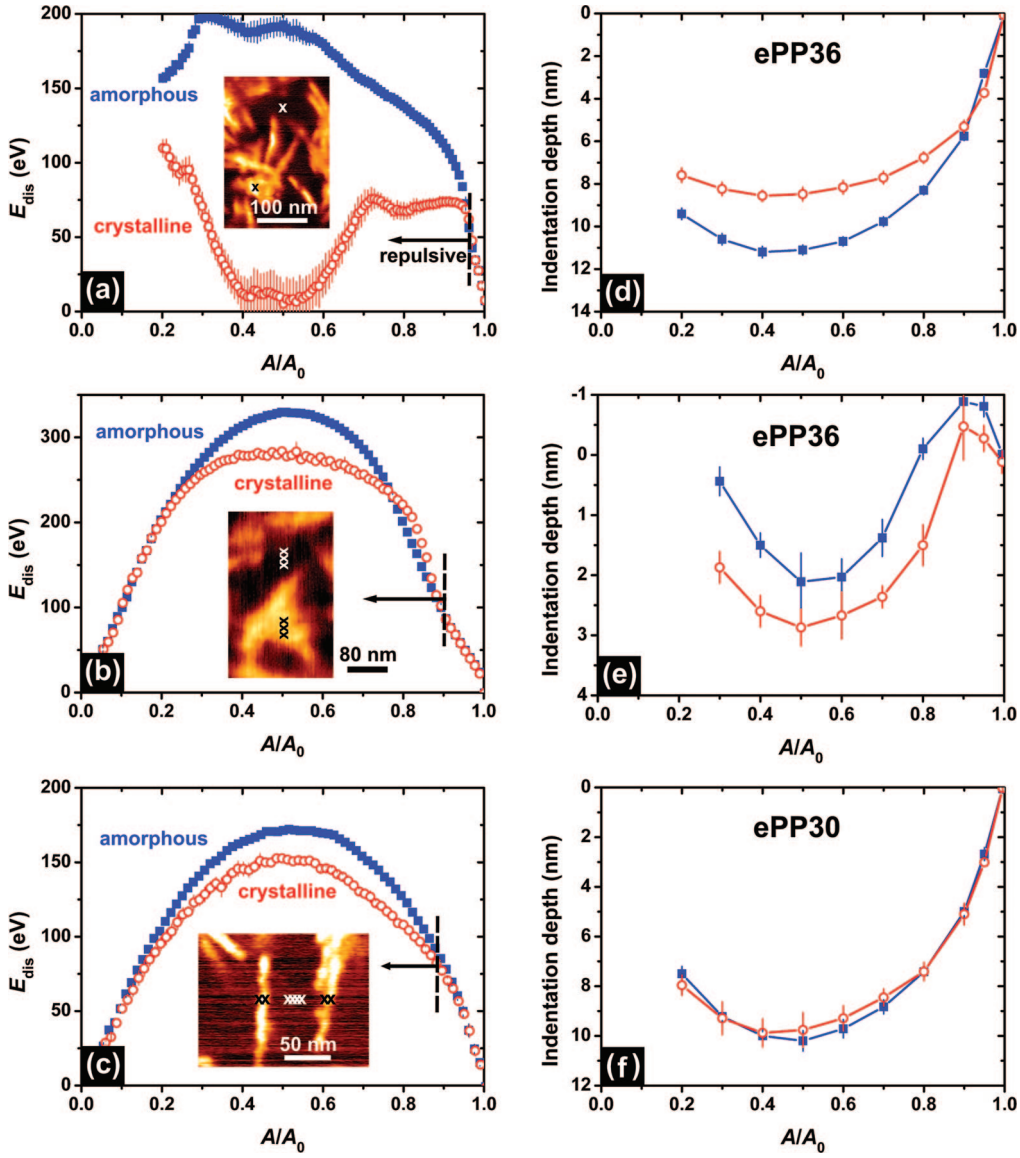

Figure 5. (a−c) Energy dissipation curves measured on amorphous (closed symbols) and crystalline (open symbols) regions of ePP36 (a, b), and ePP30 (c). The insets show AFM phase images with crosses marking the positions where the energy dissipation curves were measured. Black (white) crosses indicate positions on crystalline (amorphous) regions. (d−f) Indentation depths of the AFM tip into the sample surface versus amplitude ratio A/A_0 for amorphous and crystalline regions of ePP.

an increase of the stiffness of the surface. The similarity of the shape of both dissipation curves before etching indicates the presence of a thin (<10 nm thick) amorphous layer on top of the crystalline region, which was removed during the first etching step. After subsequent etching steps, the variation of the curves remained within the typical scatter.

Figure 4b shows the indentation depths on amorphous (blue dots) and crystalline regions (red dots) after successive etching steps at a setpoint ratio of $A/A_0 = 0.5$. Indentation depths on crystalline and amorphous regions are similar. Before etching (open symbols) the indentation is (2.5 ± 0.5) nm. The difference to the data shown in Figure 3b is attributed to differences in tip geometry. After successive etching steps (closed symbols) the indentation increases to (4.0 ± 1.0) nm. This is attributed to the etching process which chemically modifies the surface layer of ePP by oxidation of polymer chains and diffusion of molecular fragments into the polymer surface.

It is reasonable to assume that the further etching process has no significant influence on the mechanical properties of the sample surface because the indentation depths of the AFM tip into the ePP surface, the shape of the energy dissipation curves, as well as the maximum amount of dissipated energy measured on crystalline and amorphous regions remained constant.

3.5. Surface Properties for Different Materials and AFM Tips. As already shown in section 3.1, it is essential that the AFM tip hits the crystalline region at its center during the APD measurement in order to obtain a dissipation curve that differs significantly from that of an amorphous region. Parts a−c of Figure 5 show averaged dissipation curves measured on amorphous regions (closed symbols) of different ePP specimens as well as distinctive types of dissipation curves measured on crystalline regions (open symbols). The data presented in Figure 5a were obtained on ePP36. The curves are very similar to those of Figure 1. The positions where the APD curves were measured are indicated with black and white crosses on the phase images shown as inset in Figure 5a. Both curves were averaged from 20 dissipation curves. They have a characteristic shape and differ considerably in the amount of dissipated energy except for amplitude ratios in the range of $A/A_0 \approx 1.00-0.95$ where the curves resemble. Attractive interactions between the AFM tip and the surface dominate in

this range. The transition to the repulsive regime is marked by an arrow in the diagram. E_{dis} measured on the amorphous phase of the polymer increases with decreasing A/A_0 to a maximum amount of dissipated energy $E_{dis,max} = 200$ eV at a setpoint ratio $A/A_0 \approx 0.3$ and a local maximum at $A/A_0 \approx 0.5$. The dissipation curves measured on amorphous regions are within the scatter for the data sets shown (compare with Figure 1). In contrast, the dissipation curve measured on the crystalline phase is almost constant in energy for amplitude ratios $A/A_0 \approx 0.95-0.65$. It decreases rapidly for ratios around 0.5, and increases again at lower setpoint ratios ($A/A_0 \leq 0.35$). On crystalline regions of ePP the amount of dissipated energy is always lower than that on the amorphous regions.

An example for an averaged dissipation curve (obtained from three curves measured on distinctive sample positions) measured on a crystalline domain but with less deviation to the dissipation curve obtained on amorphous regions can be seen in Figure 5b. The curves correspond to the etching experiment of section 3.4 of the ePP36 sample before etching. They reveal only very small differences in both dissipation curves with respect to the maximum amount of dissipated energy. In this case, even the shape of both curves is similar and is typical for viscoelastic materials.[36]

A third example for energy dissipation curves obtained on crystalline and amorphous regions of an ePP30 sample can be seen in Figure 5(c). Although the specimen has a different degree of crystallinity, the curves look very similar to that of Figure 5(b). A further APD measurement has been accomplished on an ePP26 sample. The obtained dissipation curves (not shown) for crystalline and amorphous regions differed by $\sim$ 125 eV at maximum.

The corresponding indentation depths of the AFM cantilever into the ePP samples as a function of the amplitude ratio A/A_0 are shown in Figure 5, parts d−f, for crystalline (open symbols) and amorphous (closed symbols) regions. Figure 5d shows that the indentation monotonously increases with decreasing A/A_0 and reaches up to 11 nm on amorphous regions for the ePP36 sample shown in Figure 5a. A correlation to the kink appearing at an amplitude ratio of $A/A_0 = 0.65$ in the energy dissipation curve (Figure 5a) cannot be found in the indentation diagram. In the case of the ePP36 sample of Figure 5b and the ePP30 sample of Figure 5c, the maximal indentation depths are 3 and 10 nm at $A/A_0 = 0.5$, respectively. There is little difference in indention depths between the amorphous and the crystalline regions. For amplitude ratios $A/A_0 < 0.4$ the indentation depths decrease again with decreasing amplitude setpoint.

With these and the observations from the previous sections, we can draw the following conclusions. Indentation depths were in the range between 2−11 nm for amplitude ratios between 0.8−0.4 for all measurements independent of the specimen's degree of crystallinity. Moreover, the indentation increases with decreasing A/A_0 and decreases again at low ratios (<0.4). For the amorphous regions the maximum in tip indentation coincided with the maximum in dissipated energy. We suppose that the AFM tip additionally performs a lateral movement during the oscillation parallel to the sample surface at low amplitude ratios due to strong damping forces. However, a detailed discussion of this issue is beyond the scope of this work. Interestingly, only small deviations in indentation depths were observed for APD curves measured on crystalline and on amorphous regions for very low amplitude ratios. This is consistent with the indentation experiments of section 3.3 for the individual crystal where only 3 nm difference in the tip indentation were found between both polymer regions at an indentation depth of $\sim$ 11 nm corresponding to $A/A_0 = 0.4$ (Figure 3b).

One result of the etching experiment from the previous section is that a thin amorphous layer (thickness <10 nm) covers crystalline regions at the sample surface of ePP. A reason for the observed variations of the energy dissipation curves measured on crystalline regions could be differences in the thicknesses of this amorphous cover layer. Sakai et al.[37] claimed to have found a 3 nm thick amorphous layer on top of isotactic polypropylene (iPP). Only isotactic chains of polypropylene can form crystalline regions. Since we used elastomeric polypropylenes with a low degree of crystallinity which contains much more atactic material the amorphous cover layer might be considerably thicker than 3 nm. The thicker this amorphous layer is the smaller is the interaction between the AFM tip and the crystalline material and the larger is the viscoelastic interaction and the similarity of the dissipation curve to the curve measured on pure amorphous region. In cases of large differences between the dissipated energy measured on the amorphous and the crystalline region, the total absence of such an amorphous top layer appears reasonable. An observed difference $\Delta E_{dis} \sim 150$ eV in the amount of dissipated energy per oscillation cycle at an amplitude ratio $A/A_0 = 0.5$ of both polymer regions for the samples used in section 3.1 as well as in section 3.4 (after the etching) corroborates this hypothesis (compare $\Delta E_{dis} \approx 180$ eV in Figure 5a).

It is worth noting that shape and maximum amount of dissipated energy, as well as tip indentation varied for different cantilevers. We attribute these effects to differences of the tip apex since tip shape and radii can vary drastically for different cantilevers which in turn influences the geometry of the contact between tip and sample and hence the effective force. Apart from the free oscillation amplitude of the cantilever the Q-factor mainly controls the maximum amount of dissipated energy which varied considerably for the different measurements (see eq 1).

Considering the approach during the APD measurement, an open question is the relaxation mechanism of ePP at the sample surface. After one oscillation cycle of the cantilever movement, only the total relaxation of the sample surface into the initial state would result in the same boundary condition for the next oscillation cycle. Otherwise, a hollow at the sample surface would be formed with the ongoing approach of the AFM tip due to the compliance of the material. This could explain the larger indentation depths we observed in APD measurements compared to those during scanning. The indentation process would stop at that moment when the compressed material beneath can resist against the further penetration. Since we never observed a remanent hollow after the measurement of APD curves, we conclude that the relaxation takes place within less than a minute, which is the time needed to image the surface after performing an APD measurement. This upper limit of the relaxation time is in accordance with the observations in ref 9.

3.6. Energy Dissipation and Indentation Depth. It could be argued that differences in the E_{dis} curves between crystalline and amorphous regions of polypropylene originate from different indentation depths of the AFM tip into the polymer. In order to test this hypothesis, we determined the averaged indentation depth at a setpoint ratio of $A/A_0 = 0.5$ for all measurements on ePP26, ePP30, and ePP36 using the method of refs 33 and 38. Interestingly, the standard deviation of the averaged indentation depth for one measurement did not exceed a value of 1.4 nm although APD measurements were performed on both amorphous and crystalline regions. Figure 6 shows the maximum difference in the amount of dissipated energy between amorphous and crystalline regions as a function of the averaged indentation depth at the setpoint ratio $A/A_0 = 0.5$. Open symbols indicate measurements of etched samples. Closed squares, triangles, and dots in the diagram correspond to measurements of unetched ePP26, ePP30, and ePP36, respectively. The data points in the diagram are rather arbitrarily distributed. Hence,

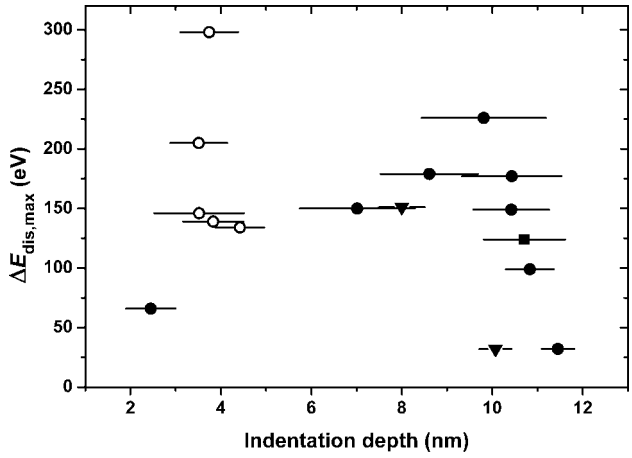

Figure 6. Maximum differences in amount of dissipated energy ΔE_{dis} between crystalline and amorphous regions as a function of the averaged indentation depth of the AFM tip at the setpoint ratio $A/A_0 = 0.5$. The standard deviation from the averaged indentation depth is shown by the error bar at each data point. In total 16 measurements are shown for different specimens taken with different cantilevers of the same type. Closed circles indicate measurements of unetched ePP36 whereas open circles indicate measurements of etched ePP36 samples. Measurements of unetched ePP26 and ePP30 are indicated by closed squares and triangles, respectively.

we conclude that there is no correlation between the maximum difference of the dissipated energy for both polymer regimes and how deep the AFM tip is indenting into the sample within the range of applied measurement parameters.

In order to figure out how the energy per oscillation cycle of the AFM tip is transferred into the surface layer, we estimated the volume of the tip apex indenting into the polypropylene surface. Only that volume can absorb the dissipated energy. The assumption of a spherical tip cap with a typical radius R_{tip} of approximately 10 nm together with an indentation depth of 10 nm, corresponds to a sphere that immerses with half of its total volume into the ePP surface. The bulk density of ePP is (0.90 $\pm$ 0.03) g/cm^3 depending on the type and crystallinity of the material[45] resulting in about 27000 monomer units per hemisphere volume. Each monomer unit contains 9 chemical bonds. In our measurement the typical amount of dissipated energy per oscillation cycle is in the order of 100 eV at an amplitude setpoint ratio $A/A_0 = 0.5$. Thus, the dissipated energy transferred to the surface layer of the specimen per oscillation cycle and per chemical bond is approximately 0.4 meV. Comparing this value with the thermal energy under ambient conditions ($T =$ 300 K) the dissipated energy converted to each chemical bond of the specimen is lower by a factor of 63. This shows that the transferred energy of the cantilever into the sample surface alone could not be sufficient for breaking chemical bonds in the material. We suppose that the indentation mechanism itself could cause deformation and flow in the material and thus can lead to the observed indentation of the tip into the sample surface.

4. Conclusions

We mapped the dissipated energy between the AFM tip and the sample surface as a function of the amplitude ratio on distinctive regions of ePP specimens with a lateral resolution of 10 nm. The dissipated energy as a function of the oscillation amplitude showed characteristic shapes for crystalline and amorphous regions of ePP. The largest differences in the amount of dissipated energy for both polymer regions occurred for amplitude ratios of the cantilever between 0.35 and 0.65. The indentation depths of the AFM tip into the ePP surface were between 2 and 11 nm and revealed only small differences between crystalline and amorphous regions. No correlation was found between the indentation depth of the AFM tip into the sample surface and the maximum difference in dissipated energy between both polymer regions. The amount of tip indentation and the change in dissipated energy upon etching led to the conclusion that an up to 10 nm thick amorphous layer covers the crystalline regions of ePP. Further etching of the specimen did not change the mechanical properties of the sample surface. Dissipation curves obtained on crystalline regions of ePP exhibited considerable variations in their shape. This could be ascribed to differences in shapes and radii of AFM tips as well as to differences in the thickness of the thin amorphous layer on top of crystalline regions. Moreover, the shape of the dissipation curves strongly depended on how close the AFM tip was located to the center of the crystalline region during the APD measurement.

In summary, we conclude that the determination of the dissipated energy as a function of the cantilever's oscillation amplitude is a sensitive probe for the detection of local mechanical surface properties of polymeric materials. This opens ways to study surface properties of a large range of heterogeneous polymeric and biological materials.

Acknowledgment. This work was financially supported by the European Commission (FORCETOOL, NMP4-CT-2004-013684) and the Volkswagen Foundation.

References and Notes

(1) Dietrich, U.; Hackmann, M.; Rieger, B.; Klinga, M.; Leskelä, M. *J. Am. Chem. Soc.* **1999**, *121*, 4348–4355.
(2) Netravali, A. N.; Caceres, J. M.; Thompson, M. O.; Renk, T. J. *J. Adhes. Sci. Technol.* **1999**, *13*, 1331–1342.
(3) Shenton, M. J.; Lovell-Hoare, M. C.; Stevens, G. C. *J. Phys. D: Appl. Phys.* **2001**, *34*, 2754–2760.
(4) Gourianova, S.; Willenbacher, N.; Kutschera, M. *Langmuir* **2005**, *21*, 5429–5438.
(5) Assender, H.; Bliznyuk, V.; Portyrakis, K. *Science* **2002**, *297*, 973–976.
(6) Granick, S.; Kumar, S. K.; Amis, E. J.; Antonietti, M.; Balazs, A. C.; Chakraborty, A. K.; Grest, G. S.; Hawker, C.; Janmey, P.; Kramer, E. J.; Nuzzo, R.; Russell, T. P.; Safinya, C. R. *J. Polym. Sci., Part B: Polym. Phys.* **2003**, *41*, 2755–2793.
(7) Fischer, H. *Macromolecules* **2002**, *35*, 3592–3595.
(8) Wang, Y.; Chan, C.-M.; Ng, K.-M.; Lin, L. *Macromolecules* **2008**, *41*, 2548–2553.
(9) Fakhraai, Z.; Forrest, J. A. *Science* **2008**, *319*, 600–604.
(10) Binnig, G.; Rohrer, H.; Gerber, Ch.; Weibel, E. *Phys. Rev. Lett.* **1982**, *49*, 57–61.
(11) Binnig, G.; Quate, C. F. Gerber, Ch. *Phys. Rev. Lett.* **1986**, *56*, 930–933.
(12) Magonov, S.; Whangbo, M. In *Surface analysis with STM and AFM*; VCH: Weinheim, Germany, 1996.
(13) Wiesendanger, R. In *Scanning probe microscopy*, Springer: Berlin, 1998.
(14) García, R.; Pérez, R. *Surf. Sci. Rep.* **2002**, *47*, 197–301.
(15) Tsukruk, V. V.; Spencer, N. D. In *Advances in scanning probe microscopy of polymers*; Wiley-VCH: Weinheim, Germany, 2001.
(16) Rehse, N.; Marr, S.; Scherdel, S.; Magerle, R. *Adv. Mater.* **2005**, *17*, 2203–2206.
(17) Dietz, C.; Röper, S.; Scherdel, S.; Bernstein, A.; Rehse, N.; Magerle, R. *Rev. Sci. Instrum.* **2007**, *78*, 053703.
(18) Franke, M.; Rehse, N. *Macromolecules* **2008**, *41*, 163–166.
(19) Dietz, C.; Zerson, M.; Riesch, C.; Gigler, A. M.; Stark, R. W.; Rehse, N.; Magerle, R. *Appl. Phys. Lett.* **2008**, *92*, 143107.
(20) Burnham, N. A.; Colton, R. J. *J. Vacuum Sci.* **1989**, *A7*, 2906–2913.
(21) Doerner, M. F.; Nix, W. D. *J. Mater. Res.* **1986**, *1*, 601–609.
(22) Oliver, W. C.; Pharr, G. M. *J. Mater. Res.* **1992**, *7*, 1564–1583.
(23) Sirghi, L.; Rossi, F. *Appl. Phys. Lett.* **2006**, *89*, 243118.
(24) Tao, N. J.; Lindsay, S. M. Lees. *S. Biophys.* **1992**, *63*, 1165–1169.
(25) Radmacher, M.; Tillman, R. W.; Fritz, M.; Gaub, H. E. *Science* **1992**, *257*, 1900–1905.
(26) Radmacher, M.; Fritz, M.; Cleveland, J. P.; Walters Hansma, P. K. *Langmuir* **1994**, *10*, 3809–3814.
(27) Heuberger, M.; Dietler, G.; Schlapbach, L. *Nanotechnology* **1994**, *5*, 12–23.
(28) Radmacher, M. *Biophys. J.* **1995**, *69*, 264–270.

(29) Radmacher, M.; Fritz, M.; Kacher, C. M.; Cleveland, J. P.; Hansma, P. K. *Biophys. J.* **1996**, *70*, 556–567.
(30) Rotsch, C.; Braet, F.; Wisse, E.; Radmacher, M. *Cell Biol. Intl.* **1997**, *21*, 685–696.
(31) Schönherr, H.; Waymouth, R. M.; Frank, C. W. *Macromolecules* **2003**, *36*, 2412–2418.
(32) Sader, J. E.; Chon, J. W. M.; Mulvaney, P. *Rev. Sci. Instrum.* **1999**, *70*, 3967–3969.
(33) Höper, R.; Gesang, T.; Possart, W.; Hennemann, O.-D.; Boseck, S. *Ultramicroscopy* **1995**, *60*, 17–24.
(34) Cleveland, J. P.; Anczykowski, B.; Schmid, A. E.; Elings, V. B. *Appl. Phys. Lett.* **1998**, *72*, 2613–2615.
(35) Tamayo, J.; García, R. *Appl. Phys. Lett.* **1998**, *73*, 2926–2928.
(36) García, R.; Gómez, C. J.; Martínez, N. F.; Patil, S.; Dietz, C.; Magerle, R. *Phys. Rev. Lett.* **2006**, *97*, 016103.
(37) Sakai, A.; Tanaka, K.; Fujii, Y.; Nagamura, T.; Kajiyama, T. *Polymer* **2005**, *46*, 429–437.
(38) Knoll, A.; Magerle, R.; Krausch, G. *Macromolecules* **2001**, *34*, 4159–4165.
(39) Boger, A.; Heise, B.; Troll, C.; Marti, O.; Rieger, B. *Eur. Polym. J.* **2007**, *43*, 3573–3586.
(40) Boger, A.; Heise, B.; Troll, C.; Marti, O.; Rieger, B. *Eur. Polym. J.* **2007**, *43*, 634–643.
(41) Carlson, E. D.; Krejchi, M. T.; Shah, C. D.; Terakawa, T.; Waymouth, R. M.; Fuller, G. G. *Macromolecules* **1998**, *31*, 5343–5351.
(42) Nony, L.; Boisgard, R.; Aimé, J. P. *J. Chem. Phys.* **1999**, *111*, 1615–1627.
(43) García, R.; San Paulo, A. *Phys. Rev. B.* **1999**, *60*, 4961–4967.
(44) García, R.; Tamayo, J.; San Paulo, A. *Surf. Interface Anal.* **1999**, *27*, 312–316.
(45) Brandrup, J.; Immergut, E. H. In *Polymer Handbook*; Wiley: New York, 1989.

MA801236P